Electronic Supplementary Material (ESI) for Inorganic Chemistry Frontiers.

Electronic Supporting Information (ESI)

Co-CeO_x Nanoparticles Anchored on Nitrogen-Doped Carbon Nanosheet: Synergistic Effect for Highly Efficient Hydrolysis of Sodium Borohydride

Longhua Yao,[a] Xiugang Li,[a] Wenfan, Peng,[a] Qilu Yao,[a] Jianhui Xia,*[b] Zhang-Hui Lu*[a]

[a]Institute of Advanced Materials, College of Chemistry and Chemical Engineering, Jiangxi Normal University, Nanchang 330022, China

[b]National Engineering Research Centre for Carbohydrate Synthesis, Jiangxi Normal University, Nanchang 330022, China

*Corresponding author: E-mail: luzh@jxnu.edu.cn

Table of Contents

Experimental section

Materials and Reagents

Cerium nitrate hexahydrate ($Ce(NO_3)_3 \cdot 6H_2O$, Aladdin, 99.95%), *cobalt* chloride hexahydrate ($CoCl_2 \cdot 6H_2O$, Aladdin, AR), potassium citrate monohydrate ($C_6H_5K_3O_7 \cdot H_2O$, Aladdin,99%), 2-Methylimidazole ($C_4H_6N_2$, Aladdin,98%)， zinc nitrate hexahydrate ($Zn(NO_3)_2 \cdot 6H_2O$, Macklin, 99%), sodium hydroxide (NaOH, Tianjin Fuchen Chemical Reagent, >96%), sodium borohydride ($NaBH_4$, Acros organics,98%), nickel chloride hexahydrate ($NiCl_2 \cdot 6H_2O$, Aladdin, 99.9%), iron(II) sulfate heptahydrate ($FeSO_4 \cdot 7H_2O$, Sinopharm Chemical Reagent Co., Ltd., 99%), copric chloride dehydrate ($CuCl_2 \cdot 2H_2O$, Aladdin, 99.99%), lanthanum(Ⅲ) nitrate hexahydrate ($La(NO)_3 \cdot 6H_2O$ Aladdin, 99%), neodymium(Ⅲ) nitrate hexahydrate ($Nd(NO)_3 \cdot 6H_2O$ Aladdin, 99.9%), yttrium(III) nitrate hexahydrate ($Y(NO)_3 \cdot 6H_2O$), and praseodymium(III) nitrate hexahydrate ($Pr(NO)_3 \cdot 6H_2O$) were used as received.

Characterization

Powder X-ray diffraction (XRD) patterns were carried out with X-ray diffractometer of Rigaku RINT-2200, using graphite monochromatized Cu Kα radiation (λ = 1.54 Å) at a scanning rate of 4°/min. An inductively coupled plasma (ICP) spectrophotometer (Varian, 725-ES) was used to determine the chemical components of the as-synthesized catalysts after the sample digested by microwave. Organic element analysis (OEA) was carried out on an EA3000 elemental analyzer (Euro EA3000, Euro Vector, Milano, Italy). The Brunauer-Emmett-Teller (BET) equation method was used to analyze the specific surface areas, on the basis of nitrogen adsorption-desorption isotherms which was recorded on a BELSORP-mini II at 77 K. X-ray photoelectron spectroscopy (XPS) analyses were carried out on an ESCALAB 250XI X-ray photoelectron spectrometer using an Al Kα source. Transmission electron microscopy (TEM) and scanning transmission electron microscopy (STEM) images and energy-dispersive X-ray spectroscopy (EDS) mapping analyses were recorded on SU-8020 and JEM-2100 with Super-X EDS system under operating voltages of 300

kV.

Synthesis of ZIF-8

ZIF-8 is synthesized according to previous literature.[47] Typically, 10 mmol $Zn(NO_3)_2 \cdot 6H_2O$ and 80mmol 2-methylimidazole is dispersed in 40ml methanol respectively. The zinc nitrate solution was added dropwise to the 2-methylimidazole solution, standing for 24 hours at room temperature, The white precipitate was separated by centrifugation and washed with methanol several times. After drying in a vacuum oven at 333 K overnight, the resulting white solid powder is the ZIF-8. As shown in SEM, the as-synthesized ZIF-8 shows a uniform rhombic dodecahedron structure.

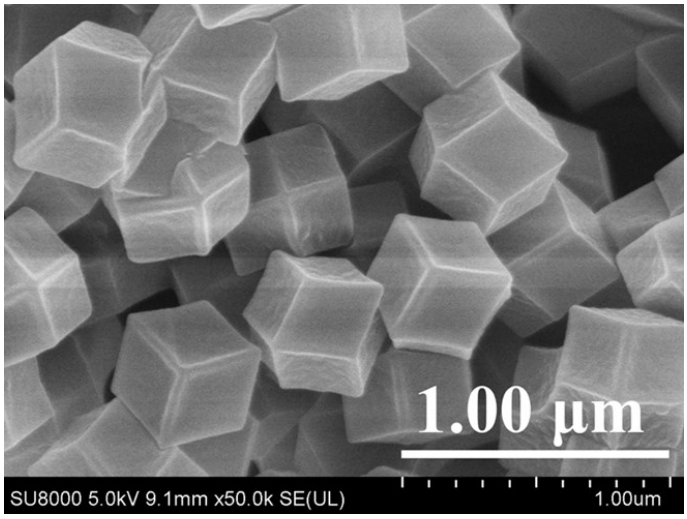

SEM image of the as-synthesized ZIF-8.

Calculation methods

The Hydrogen generation rate (HGR) is based on the mass of Co, which was calculated from the equation below:

$$HGR = \frac{V_{H2}}{m_{Co} t_{min}}$$

In the equation, V_{H2} is the total volume of generated H_2, m_{Co} is the mass of Co atoms in catalyst, and t_{min} is the completion time of the reaction in minute.

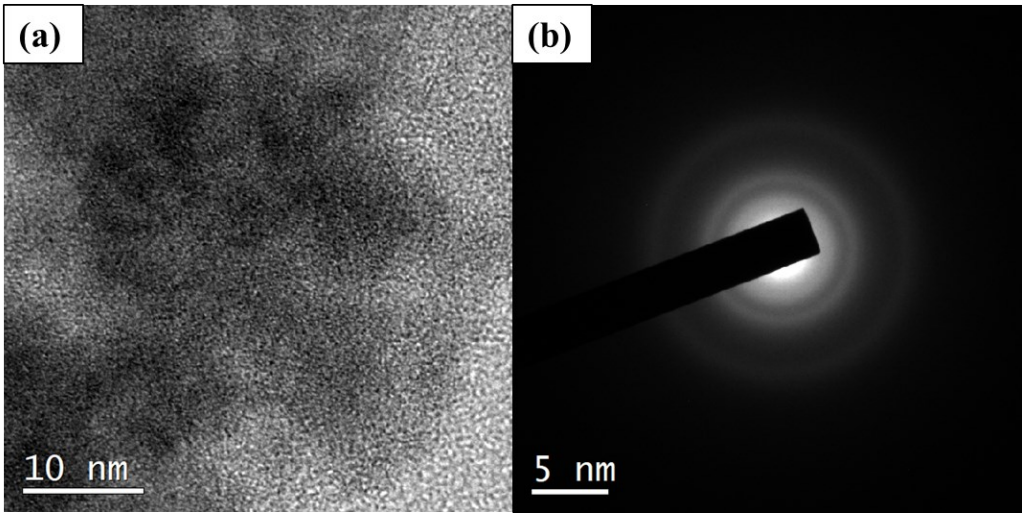

Figure S1 HRTEM and corresponding SAED pattern of Co-CeO_x/NCNS.

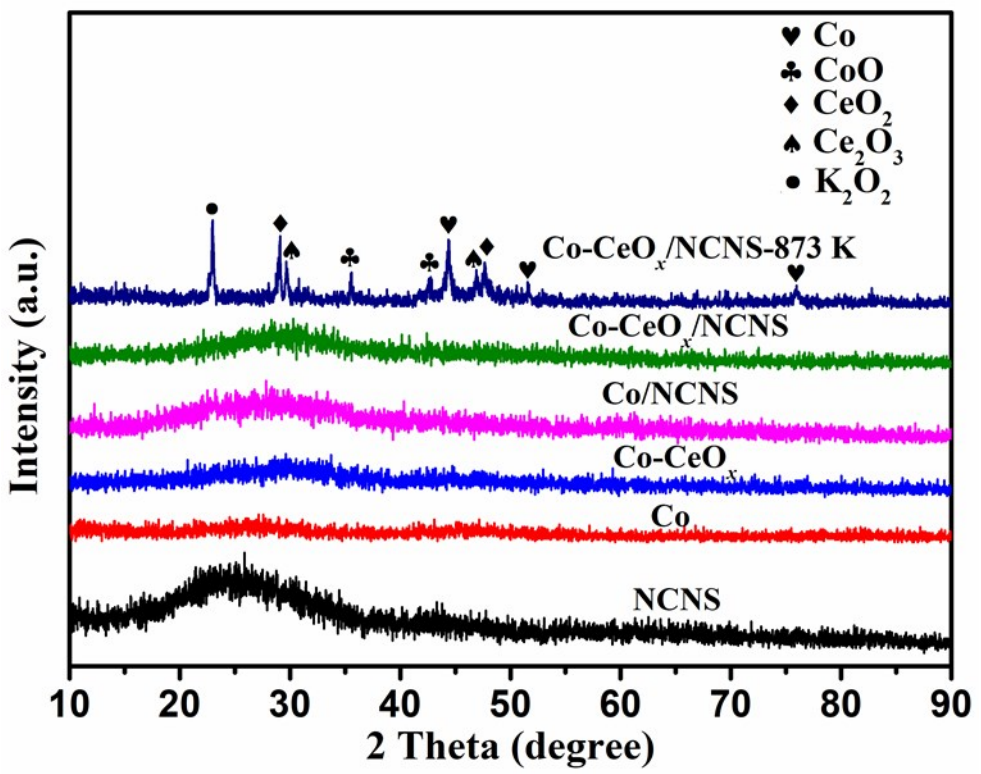

Figure S2 X-ray diffraction patterns for the NCNS, Co, Co-CeO_x, Co/NCNS, Co-CeO_x/NCNS, and Co-CeO_x/NCNS annealed at 773 K for 4 h under Ar in tube furnace.

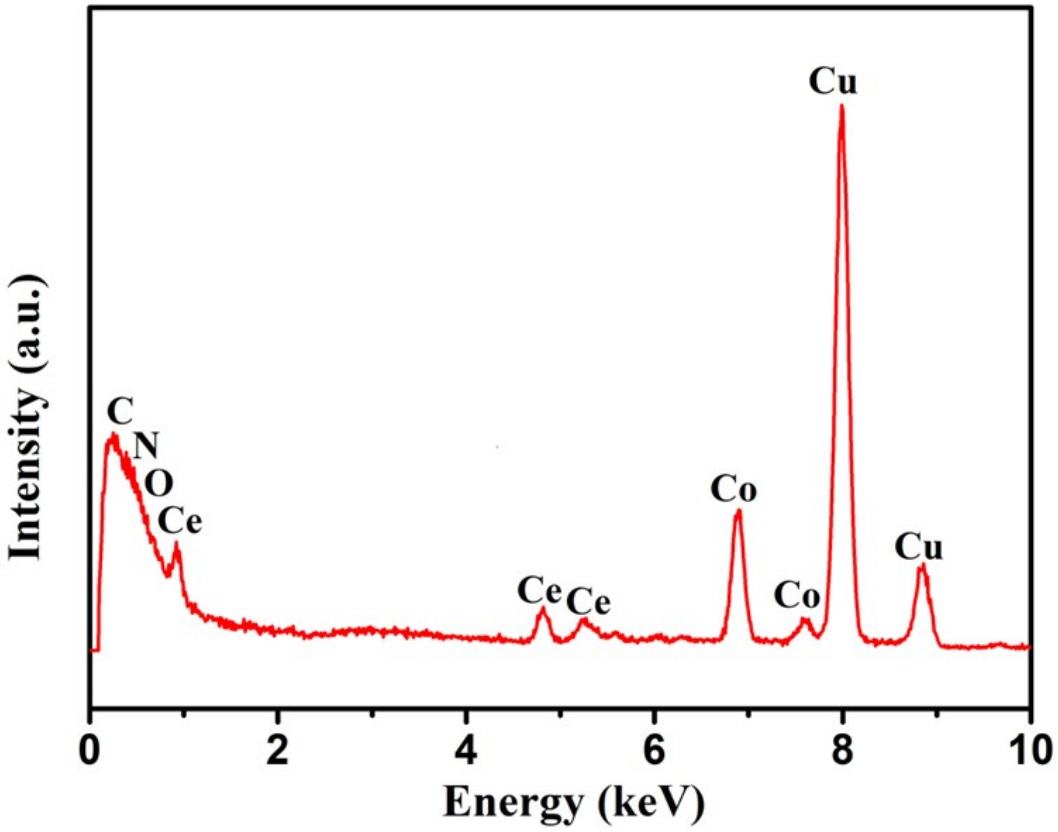

Figure S3 EDX pattern of Co-CeO_x/NCNS.

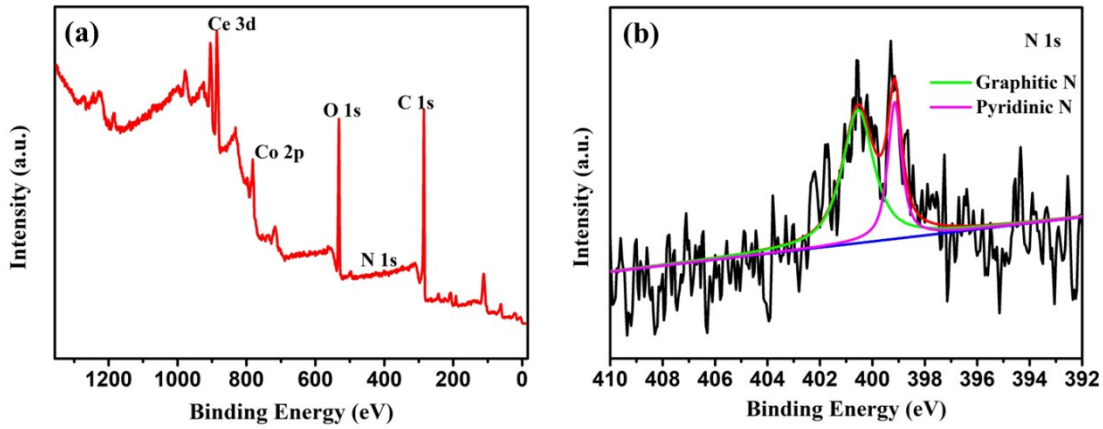

Figure S4 (a) the survey XPS spectrum and (b) XPS spectrum of N 1s of Co-CeO_x/NCNS.

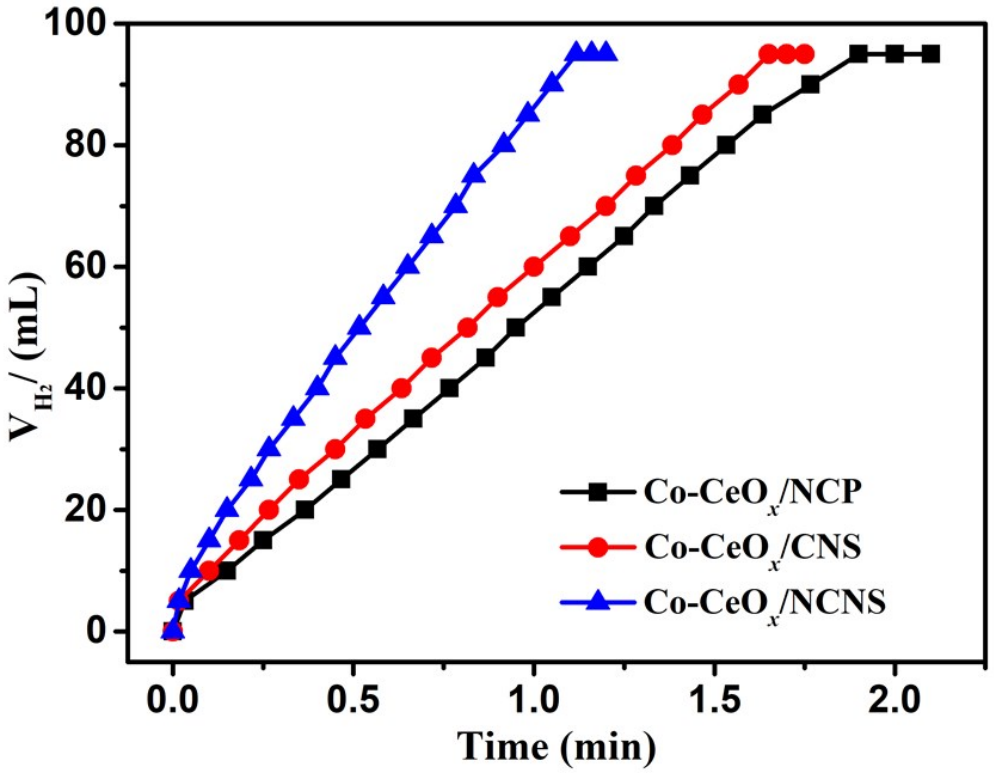

Figure S5 Time plots for hydrogen release from $NaBH_4$ (200mM, 5mL) catalyzed by Co-CeO_x/NCNS, Co-CeO_x/NCP, and Co-CeO_x/CNS respectively.

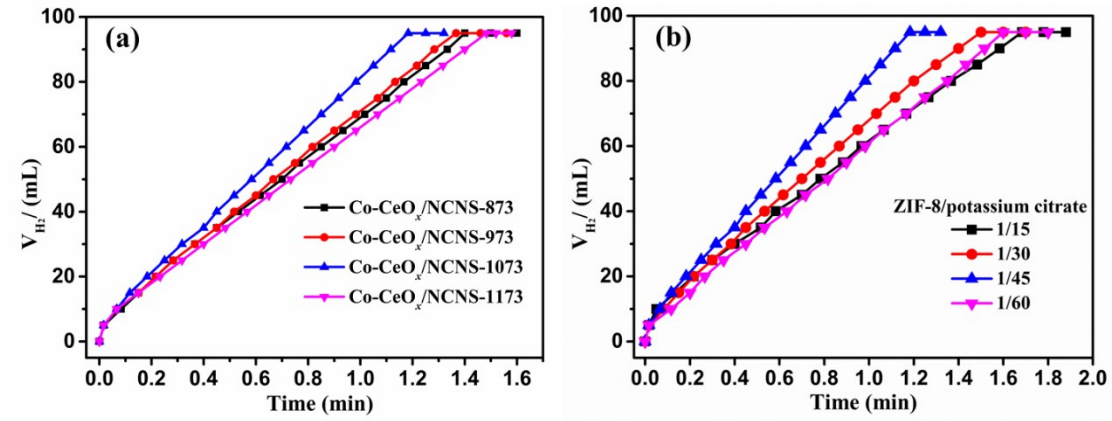

Figure S6 Time plots for hydrogen release from $NaBH_4$ (200mM, 5mL) catalyzed by Co-CeO_x/NCNS (a) synthesized by varying different temperatures and (b) different precursors of ratio (ZIF-8/potassium citrate) at 303 K (c_{NaOH}=0.4 M, n_{Co}=0.05 mmol).

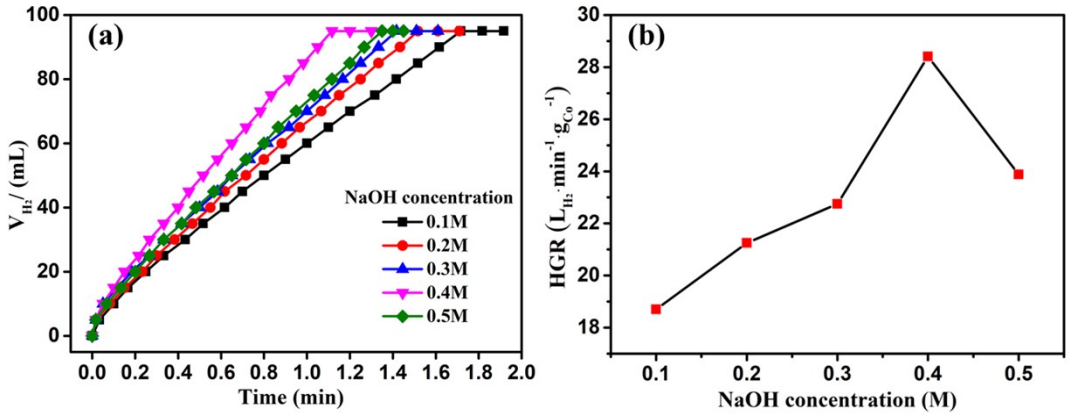

Figure S7 (a) Volume of the generated hydrogen versus time and (b) corresponding HGR for $NaBH_4$ dehydrogenation over Co-CeO_x/NCNS catalysts with different NaOH concentration at 303 K.

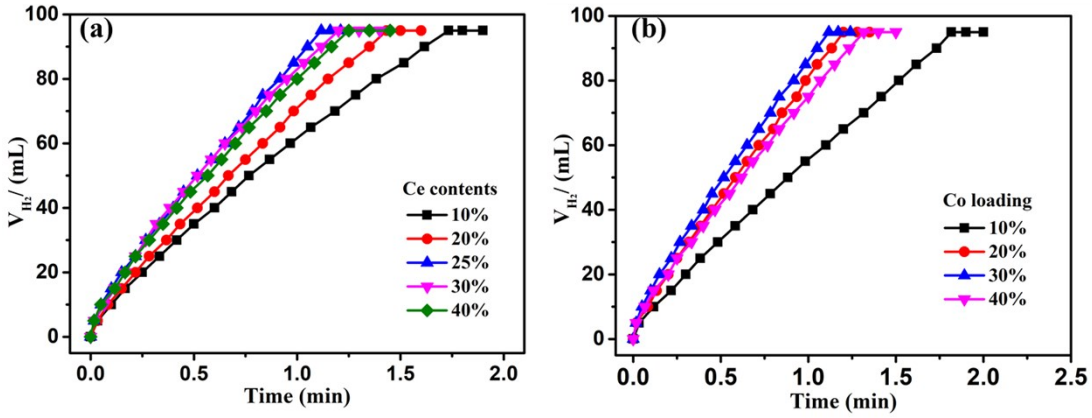

Figure S8 Time plots for hydrogen release from $NaBH_4$ (200mM, 5mL) catalyzed by Co-CeO_x/NCNS with (a) different molar ratio of n_{Ce}/n_{Co+Ce}, (b) different Co loadings at 303 K (c_{NaOH}=0.4 M, n_{Co}=0.05 mmol).

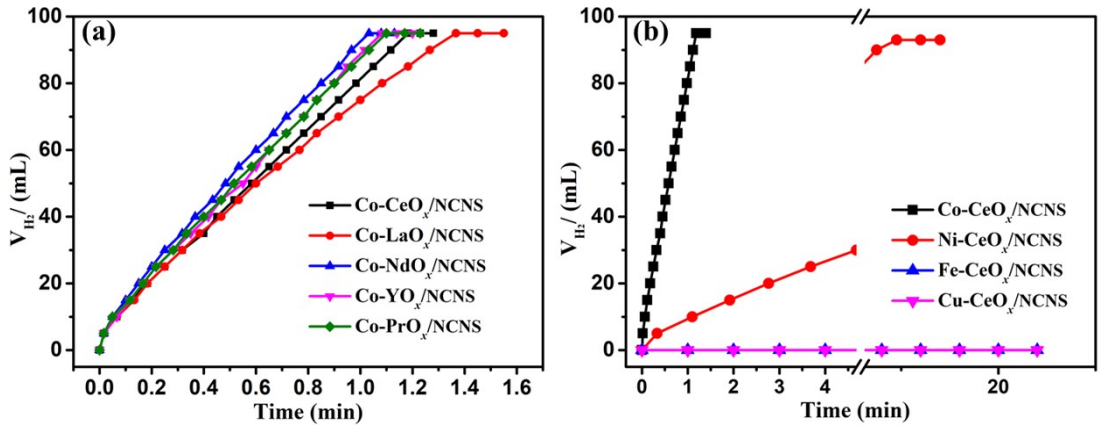

Figure S9 Time plots for hydrogen release from $NaBH_4$ (200mM, 5mL) catalyzed by (a) Co-RO_x/NCNS (R = Ce, La, Nd, Y, Pr) and (b) M-CeO_x/NCNS (M = Co, Ni, Fe, Cu) at 303 K (c_{NaOH}=0.4 M, n_{Co}=0.05 mmol).

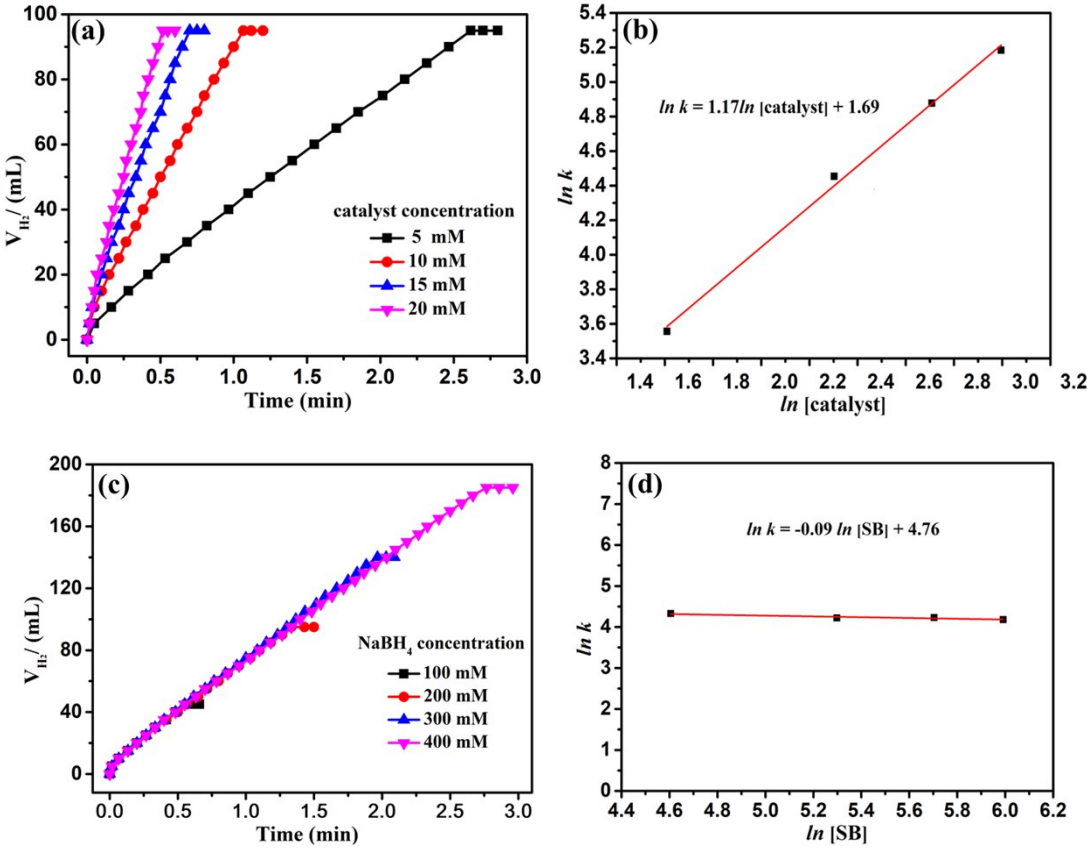

Figure S10 Time plots for hydrogen release from $NaBH_4$ catalyzed by Co-CeO_x/NCNS with (a) different catalyst concentration, and (c) different $NaBH_4$ concentration. Plot of the hydrogen generation rate versus (b) metal concentration and (d) $NaBH_4$ concentration, respectively, both in logarithmic scale.

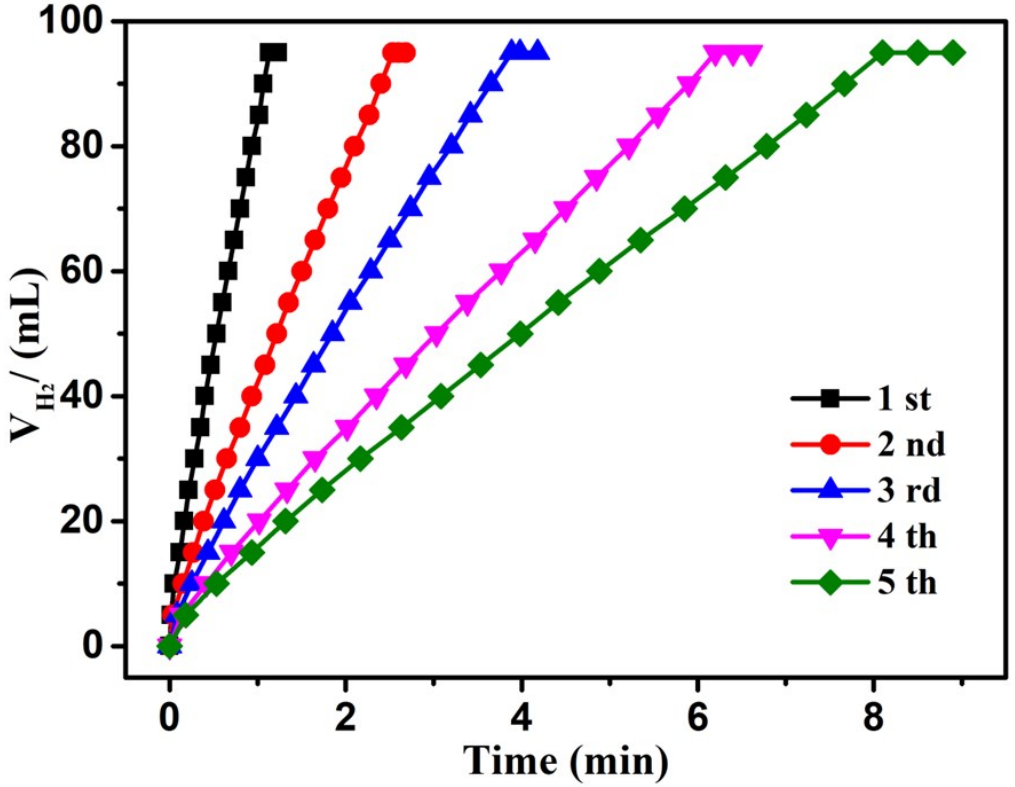

Figure S11 Stability test for H_2 release from $NaBH_4$ over the Co-CeO_x/NCNS catalyst with NaOH (c_{NaOH}=0.4 M, n_{Co}=0.05 mmol) at 303 K.

Table S1 ICP-AES results for the as-synthesized Co-CeO_x/NCNS catalysts.

Catalysts loading	Co (wt %) : Ce (wt %)	Co : Ce (atomic ratio)
10% Co-CeO_x/NCNS	9.21 : 7.51	0.0467 : 0.0160
20% Co-CeO_x/NCNS	20.42 : 16.29	0.0493 : 0.0165
30% Co-CeO_x/NCNS	27.84 : 22.12	0.0497 : 0.0166
40% Co-CeO_x/NCNS	36.29 : 28.85	0.0498 : 0.0166

Table S2 Comparison of HGR and activation energy (E_a) in this study with those reported in previous studies.

catalyst	reation temperature (K)	HGR ($mL_{H_2}\cdot min^{-1}\cdot g_M^{-1}$)	E_a ($kJ\cdot mol^{-1}$))	Ref.
Co@ZIF-8	303	14000	62.9	42
Co@C_2N-h2D	303	31238[b]	66.174	13
Co-Mo/3DGO	298	7023	35.6	26
Porous Co_3O_4	298	19520[b]	–[a]	S2
Porous Co-B nanoalloy	303	6284[b]	30	S3
Co/PGO	298	5955	55.22	S4
Co-B/C	298	1127[b]	57.8	S5
Co@C-700	303	–[a]	56.9	S6
dandelion-like Co-Mo-B	303	20298[b]	51	S7
Co–Zn/Ni	298	576[b]	50.2	S8
Co–P	303	3300	60.2	S9
Ni-B–silica nanocomposite	298	1916[b]	60.7	S10
NiB/$NiFe_2O_4$	298	2999[b]	72.52	S11
Cu–B	303	6500[b]	23.79	S12
Co-CeO_x/NCNS	303	28410	44.16	**This work**

a. Not reported or no detailed data are available.

b. HGR value is calculated according to the active component.

Reference

(S1) Chen, Y. Z.; Wang, C.; Wu, Z. Y.; Xiong, Y.; Xu, Q.; Yu, S. H.; Jiang, H. L. From Bimetallic Metal-Organic Framework to Porous Carbon: High Surface Area and Multicomponent Active Dopants for Excellent Electrocatalysis. *Adv. Mater.* **2015**, 27 (34), 5010-6

(S2) Ma, M.; Wei, L.; Jin, F. Porous Co_3O_4 nanoplatelets as efficient catalyst precursor for hydrogen generation from the hydrolysis of alkaline sodium borohydride solution. *Funct. Mater. Lett.* **2019**, 12 (01), 1850109.

(S3) Wang, X.; Liao, J.; Li, H.; Wang, H.; Wang, R.; Pollet, B. G.; Ji, S. Highly active porous Co–B nanoalloy synthesized on liquid-gas interface for hydrolysis of sodium borohydride. *Int. J. Hydrogen Energy*, **2018**, 43 (37), 17543-17555.

(S4) Zhang, H.; Feng, X.; Cheng, L.; Hou, X.; Li, Y.; Han, S. Non-noble Co anchored on nanoporous graphene oxide, as an efficient and long-life catalyst for hydrogen generation from sodium borohydride, *Colloid. Surface A*. **2019**, 563, 112-119.

(S5) Zhao, J.; Ma, H.; Chen, J. Improved hydrogen generation from alkaline $NaBH_4$ solution using carbon-supported Co–B as catalysts. *Int. J. Hydrogen Energy*. 2007, 32 (18), 4711-4716.

(S6) Zhang, X.; Sun, X.; Xu, D.; Tao, X.; Dai, P.; Guo, Q.; Liu, X. Synthesis of MOF-derived Co@C composites and application for efficient hydrolysis of sodium borohydride, *Appl. Surf. Sci.*, **2019**, 469, 764-769.

(S7) Wei, Y.; Wang, R.; Meng, L.; Wang, Y.; Li, G.; Xin, S.; Zhao, X.; Zhang, K. *Int. J. Hydrogen Energy*. **2017**, 42 (15), 9945-9951.

(S8) Wei, L.; Ma, M.; Lu, Y.; Zhang, S.; Gao, J.; Dong, X. Electrodeposited Co–Zn on Ni foam as efficient catalysts for hydrogen generation from hydrolysis of sodium borohydride, *Funct. Mater. Lett.*, **2017**, 10 (05), 1750065.

(S9) Eom, K.; Cho, K.; Kwon, H. Effects of electroless deposition conditions on microstructures of cobalt–phosphorous catalysts and their hydrogen generation properties in alkaline sodium borohydride solution. *J. Power Sources*, **2008**, 180 (1), 484-490.

(S10) Chen, Y.; Kim, H. Use of a nickel-boride–silica nanocomposite catalyst prepared by in-situ reduction for hydrogen production from hydrolysis of sodium borohydride. *Fuel Process. Technol.* **2008**, *89* (10), 966-972.

(S11) Liang, Z.; Li, Q.; Li, F.; Zhao, S.; Xia, X. Hydrogen generation from hydrolysis of $NaBH_4$ based on high stable $NiB/NiFe_2O_4$ catalyst. *Int. J. Hydrogen Energy*. **2017**,

42 (7), 3971-3980.

(S12) Bekirogullari, M. Catalytic activities of non-noble metal catalysts (Cu-B, Fe-B, and Ni-B) with C.Vulgaris microalgal strain support modified by using phosphoric acid for hydrogen generation from sodium borohydride methanolysis. *Int. J. Hydrogen Energy*. **2019,** *44* (29), 14981-14991.